PERGAMON

International Journal of Heat and Mass Transfer 44 (2001) 1627–1636

International Journal of HEAT and MASS TRANSFER

www.elsevier.com/locate/ijhmt

Enhanced laminar-flow heat transfer at fiber-flocked surfaces

Kurt O. Lund [a,*], Timothy R. Knowles [b]

[a] *Department of Mechanical and Aerospace Engineering, Center for Energy Research, Jacobs School of Engineering, University of California, La Jolla, CA 92093-0417, USA*

[b] *Energy Science Laboratories, Inc., 6888 Nancy Ridge Drive, San Diego, CA 92121-2233, USA*

Received 20 October 1999; received in revised form 20 April 2000

Abstract

High-conductivity carbon fibers have been "flocked", or perpendicularly attached onto surfaces, thus enabling heat transfer enhancement for such fiber-flocked surfaces. Here, an analysis is performed for fully developed laminar flow and heat transfer in plane and cylindrical ducts with fiber-covered walls. The fiber volumetric packing density is sparse such that single-cylinder correlations are applied for the drag and heat transfer between the fibers and the fluid; this gives rise to body-type terms in the momentum and energy equations for the fiber region near the wall. These equations are solved by singular perturbation theory, and matched to the core flow without fibers.

The result of this analysis is in terms of friction factor and Nusselt number multipliers, which are constant for all laminar Reynolds numbers, but which vary strongly with the length of the fibers relative to the duct half-width or radius. For large fiber conductivities and relative lengths, the results indicate a greater heat transfer enhancement than hitherto possible.

1. Introduction

1.1. Technology significance

In the present work we consider the fully developed laminar flow and heat transfer in circular and planar ducts having surfaces sparsely covered with filaments (fibers or hairs). For example, carbon-fiber filaments may be *flocked* onto the surface, but limited to the wall region of the shear flow, which normally has the largest velocity and temperature gradients (i.e., largest friction and heat-flow resistance). Therefore, placement of high-conductivity fibers in this region has the capacity of reducing the wall thermal resistance, thus enhancing the surface heat transfer capability.

Electric and pneumatic flocking techniques can be used to arrange large numbers of fibers perpendicular to surfaces, thus producing micro-finned surfaces for enhanced heat transfer, as shown in Fig. 1(a). Such flocked tube and plate configurations using ~10 μm carbon fibers have been fabricated with fiber lengths in the range of 0.1–10 mm, with volume packing densities in the range of 0.1–20%, and with fiber conductivities as high as 1100 W/mK. Although the fiber packing in the Fig. 1(a) photograph appears dense, this is an optical illusion since the packing here is only 2%.

For metallic substrates the fibers are typically embedded in a layer of conductive adhesive that is several fiber-diameters thick, such that the wall ends of the fibers contact the metal substrate through the adhesive; the observed wall-unit thermal conductance associated with this contact is typically ~2000 W/m^2 K for a 1% packing density and 10 μm fibers. For high-flux applications the fibers can be embedded directly in a metallic substrate by soldering or electro-forming, or incorporated in carbon plates or tubing for applications where lighter weight and higher temperature capability are required.

1.2. Previous work

Previous investigations of flow and heat transfer at fiber-covered surfaces have been for application to mammals covered with hair [1,2], and have been concerned with insulating properties. In these studies, the

* Corresponding author.

0017-9310/01/$ - see front matter
PII: S0017-9310(00)00205-2

Nomenclature

A	area
B	wall-to-centerline distance
C_D	fiber drag coefficient
C_p	fluid specific heat
D	duct diameter, hydraulic diameter
d	fiber diameter
F	heat-flux parameter
f	friction factor
f_D	volumetric fiber drag force
H	fiber length (height above wall)
h	fiber-surface heat transfer coefficient
h_A	bulk-average heat transfer coefficient
h_c	fiber/wall contact conductance
k	thermal conductivity
K	pressure-gradient parameter
m_f	friction factor multiplier, $m_f = f/f_{smooth}$
m_h	Nusselt number multiplier, $m_h = Nu/Nu_{smooth}$
Nu_A	bulk Nusselt number, $h_A D/k_g = [q_W/(T_W - T_A)]D/k_g$
Nu_d	fiber-diameter Nusselt number, hd/k_g
n	shape index ($=1$ for circular, $=0$ for planar), exponent
P	perimeter
p	pressure
Pr	Prandtl number, $C_p\mu/k_g$
q	heat flux
R	radial distance from centerline
R_W	radius of the duct ($=B$)
Re	duct Reynolds number, $\rho U_A D/\mu$
Re_H	H-Reynolds number, $\rho U_H H/\mu$
r_s	conductance ratio, $\sigma k_s/(1-\sigma)k_g$
S	fiber/wall contact shape factor
T	temperature
U	axial velocity
u	nondimensional axial velocity, U/U_H
u_A	nondimensional duct-average axial velocity, U_A/U_H
X	axial coordinate
Y	transverse coordinate (distance from wall)
y	nondimensional coordinate, Y/H

Greek symbols

α	fluid thermal diffusivity
β	duct-width/fiber-length ratio, B/H
δ	fiber slenderness (d/H)
ε	perturbation parameter
γ	convective parameter
η	velocity inner coordinate, $(1-y)/\varepsilon$ or y/ε
κ	conductivity ratio, k_g/k_s
λ	fiber drag constant, $(\delta Re_H)^{3/4}/10$
μ	viscosity
θ	scaled temperature, $[T - T_W]/[T_H - T_W]$
ρ	fluid density
σ	fiber packing fraction (volumetric fraction of solid)
τ	shear stress
ψ	re-scaled temperature, θ/F
ζ	thermal inner coordinate, $(1-y)/\delta$
ω	flow parameter, $\omega^2 = 5/2^{9/4} \approx 1.05$
Ω	thermal parameter, $2\sqrt{[Nu_d\kappa(1+r_s)]}$

Subscripts

A	mixing-cup bulk-average for entire duct
C	fiber-free core
c	fiber/wall contact
D	fiber drag
g	fluid (gas)
H	evaluation at $Y = H$ (tip of fibers)
m	mean value over core, only
s	solid (fibers)
W, w	wall

hair filaments are comparatively long with dense packing, so that porous-media flow was used as a modeling basis, including uniform flow throughout the medium [1]. These models are not applicable to the present sparse-packing conditions that concern enhanced heat transfer. Instead, we consider single-filament correlations to apply to the flow and temperature fields between the filaments. Other recent studies have considered various "interrupted" surfaces [3], and rectangular rib-roughness surfaces [4].

1.3. Present approach

In this work, the laminar flow and heat transfer near the fiber-covered surface are determined. Appropriate resistance and convection laws are reviewed for application to sparse packing of very thin cylinders (fibers); these are integrated into the descriptive differential equations of the fiber region. Solution of these equations and matching to the core conditions result in friction factors and Nusselt numbers which depend on the fiber properties and geometries. It is shown that substantial heat transfer improvement is possible for fully developed laminar flow, albeit at the expense of increased flow resistance. This stands in contrast to conventional surface augmentation methods which have limited heat transfer enhancements in laminar and transitional flows [3,4]. The analysis is applicable to planar ($n = 0$) and circular ($n = 1$) ducts, but with fibers limited to the wall region for the circular geometry.

2. Problem formulation

To investigate the benefits of fiber-enhanced surfaces, fully developed flow and heat transfer are considered

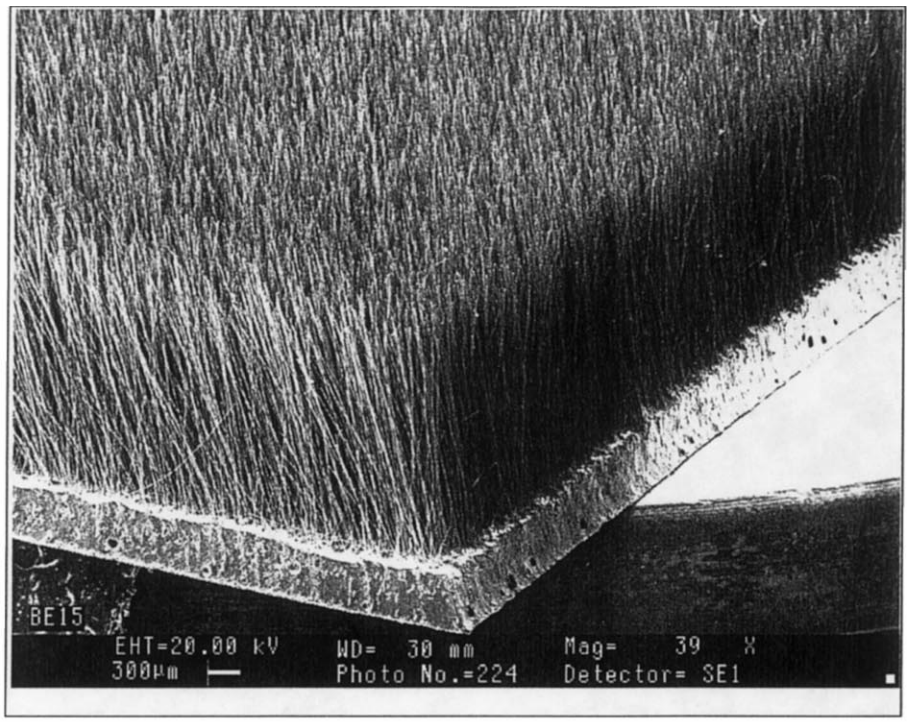

(a)

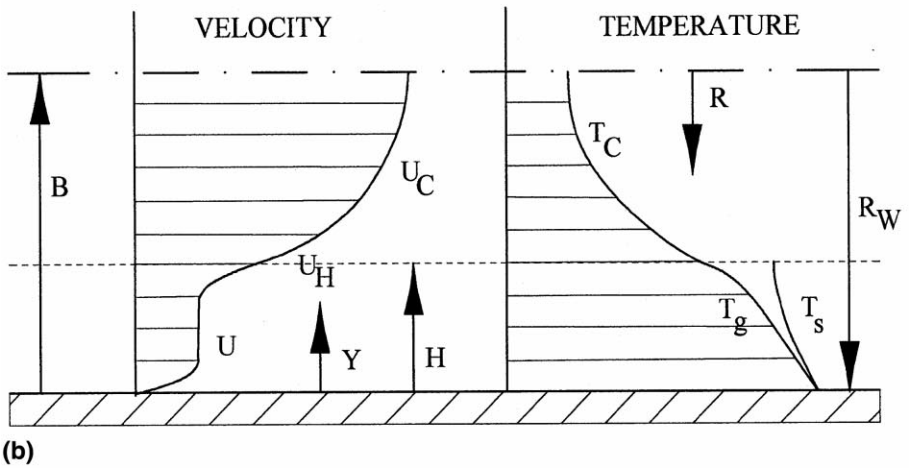

(b)

Fig. 1. (a) Micro-photograph of typical carbon fibers flocked onto a substrate (courtesy, Energy Science Laboratories, Inc.). (b) Definition diagram for velocity and temperature fields.

here for circular ducts with radius R_W and planar ducts of half-width B, and having fiber region height H, as shown in Fig. 1(b). Then, in the core region, $0 \leqslant R \leqslant R_W - H$, or $H \leqslant Y \leqslant B$, the velocity and temperature fields have zero slopes on the centerline, and have the respective velocity and temperature values U_H and T_H at the interface, $Y = H$; additionally, in the fiber region, $0 \leqslant Y \leqslant H$, the velocity is zero at the wall, where the constant wall heat flux is specified as q_W. The unknown quantities, U_H and T_H, are determined subsequently from the matching of shear stresses and heat fluxes at the interface. We denote averages over the entire duct cross-section with subscript A, and those for the core region only with subscript m.

2.1. Fiber region velocity

Consider a surface flocked with fibers of height H and diameter d, as shown in Fig. 1(b), with fibers restricted to the near-planar wall region. Above the fibers there is flow which results in axial velocity U_H at the tip of the fibers at $Y = H$. For a differential volume at distance Y from the wall, a force balance yields the following:

$$(1-\sigma)\frac{\partial \tau}{\partial Y} - f_D = -\left(-\frac{\partial p}{\partial X}\right) \equiv -\frac{1}{2}\rho U_H^2 \frac{f_H}{H} = -\frac{1}{2}\rho U_A^2 \frac{f}{D}, \tag{1a}$$

where $f_D = 2\sigma\rho U^2 C_D/(\pi d)$ is the drag force per unit volume due to the fibers and f_H is the H-friction factor defined by the pressure gradient in (1a); the usual Darcy friction factor is defined in terms of the average velocity, U_A, and hydraulic diameter, D. Let $u = U/U_H$ and $y = Y/H$; then, the stress–viscosity relationship $\tau = \mu\partial U/\partial Y$, and multiplying through by $H/\rho U_H^2$, results in the nondimensional equation:

$$\frac{(1-\sigma)}{Re_H}\frac{d^2u}{dy^2} - \frac{2\sigma}{\pi\delta}u^2 C_D = -\frac{f_H}{2}, \tag{1b}$$

where $u(0) = 0$ and $u(1) = 1$, or $U(H) = U_H$; here the H-Reynolds number, $Re_H = \rho U_H H/\mu$, and the fiber slenderness ratio, $\delta = d/H$, are both small quantities.

Drag coefficients for larger circular cylinders in cross-flow are reported graphically [5], and for small fiber Reynolds numbers they are available from the Oseen analytical solution [6]; however, the Oseen solution is singular for $Re_d > 1$, and beyond this value there are no analytical solutions. Fowler and Bejan [2] present a transverse-flow, porous-medium permeability of $K_p = d^2/125\sigma^{1.6}$, which results in an equivalent single-cylinder drag coefficient of $C_D = 125\pi\sigma^{0.6}/Re_d$; however, for sparse packing, this result is not in agreement with single-cylinder data. White [6] presents a correlation of the experimental data from fine, hot-wire anemometer wires, which with $n \approx 2/3$ is valid over a large Reynolds number range:

$$C_D = 1 + \frac{10}{Re_d^n} = 1 + \frac{10}{(\delta Re_H u)^n} = \frac{10}{(\delta Re_H)^n}\left(u^{-n} + \frac{(\delta Re_H)^n}{10}\right) \equiv \frac{1}{\lambda}(u^{-n} + \lambda). \tag{2}$$

Here, to achieve better agreement with the Oseen theory for small $Re_d = \delta Re_H u(y)$, the exponent in (2) is taken as $n = 3/4$, and $\lambda \equiv (\delta Re_H)^{3/4}/10 \ll 1$. These correlations are illustrated in Fig. 2(a), where it is seen that the present correlation (2) agrees with the Oseen theory and the White correlation. Because of the small fiber diameters, the fiber-diameter Reynolds numbers tend to be small. Substitution of (2) into (1b) then yields the momentum equation:

$$\varepsilon^2\frac{d^2u}{dy^2} - \left(u^{5/4} + \lambda u^2\right) = -\varepsilon^2\frac{f_H Re_H}{2(1-\sigma)} \equiv -\varepsilon K_H, \tag{3a}$$

where the leading multiplier is a small parameter:

$$\varepsilon \equiv \sqrt{\frac{\pi(1-\sigma)\delta^2}{20\sigma(\delta Re_H)^{1/4}}} = \frac{\delta}{2}\sqrt{\frac{\pi(1-\sigma)}{5\sigma(\delta Re_H)^{1/4}}} \prec\prec 1. \tag{3b}$$

That is, we limit investigation to the practical cases of small fiber slenderness ratios (e.g. $\delta < 0.01$), such that $\varepsilon < 0.3$. Since $0 \leqslant u \leqslant 1$, it is convenient for the analytical solution of (3a) to expand the drag force in a Taylor series about $u = 1/2$. Thus, considering that λ is small, (3a) is written as

$$\varepsilon^2\frac{d^2u}{dy^2} - \omega^2 u = -\frac{1}{8\times 2^{1/4}} - \varepsilon K_H + \frac{\lambda}{4} \equiv -\omega^2 K_L, \tag{3c}$$

where $\omega^2 = 5/(4\times 2^{1/4}) \approx 1.05$, and $K_L = 1/10 + (\varepsilon K_H - \lambda/4)/\omega^2$; in (3c), K_L (or K_H) is a parameter to be determined from the solution, and from which the friction factor is derived.

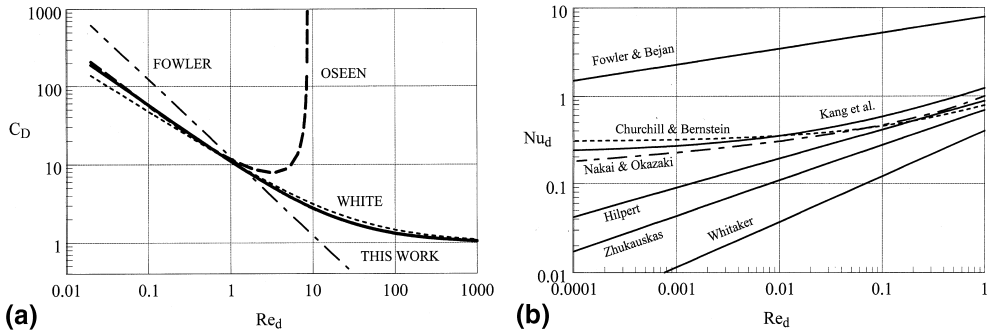

Fig. 2. (a) Comparison of drag-coefficient correlations. (b) Comparison of fiber-diameter Nusselt number orrelations for $Pr = 0.7$.

2.2. Central core region velocity

In the fiber-free central region of a *circular* duct, the laminar flow equation is

$$\frac{\mu}{R}\frac{\partial}{\partial R}\left\{R\frac{\partial U_C}{\partial R}\right\} = -\frac{1}{2}\rho U_H^2\frac{f_H}{H} = -\frac{1}{2}\rho U_A^2\frac{f}{D} \tag{4a}$$

where $R = R_W - Y = H(\beta - y)$. In variables scaled by U_H and H, (4a) is

$$\frac{1}{(\beta-y)^n}\frac{\partial}{\partial y}\left\{(\beta-y)^n\frac{\partial u_C}{\partial y}\right\} = -\frac{1}{2}Re_H f_H,$$
$$n = \begin{cases} 0, & \text{planar} \\ 1, & \text{circular} \end{cases} \tag{4b}$$

with zero slope at $y = \beta(R = 0)$ and $u_C(1) = 1$. The average velocity for the entire cross-section is then given by

$$\frac{U_A}{U_H} \equiv u_A = \frac{2^n}{\beta}\left\{\int_0^1 u\,dy + \int_1^\beta u_C(1 - y/\beta)^n\,dy\right\}. \tag{5}$$

2.3. Fiber region heat transfer

In a similar manner, at distance Y, energy balances on fiber (solid) and fluid (gas) control volumes yield the following equations:

$$A_s\frac{\partial q_s}{\partial Y} = P_s q_{gs} = hP_s(T_g - T_s), \tag{6a}$$

$$A_g\frac{\partial q_g}{\partial Y} = -P_s q_{gs} - \rho C_p A_g\frac{\partial UT_g}{\partial X}, \tag{6b}$$

where q_{gs} is the heat flux from the gas to the solid, P_s the total fiber perimeter in the control volume and A refers to the total area, parallel to the wall. Or, with $U \neq U(X)$ and the Fourier conduction relationship, $q = -k\partial T/\partial Y$, the energy equations are obtained

$$\frac{\partial^2 T_s}{\partial Y^2} - \frac{hP_s}{k_s A_s}(T_s - T_g) = 0, \tag{7a}$$

$$\frac{\partial^2 T_g}{\partial Y^2} - \frac{hP_s}{k_g A_g}(T_g - T_s) = \frac{U}{\alpha_g}\frac{\partial T_g}{\partial X}, \tag{7b}$$

where h is the heat transfer coefficient between the fluid and the fibers at distance Y. Eq. (7a) is recognized as the thermal fin equation [7], and (7b) as the modified laminar convection equation [8]. Let nondimensional temperatures be defined by $\theta = [T - T_W(X)]/[T_H(X) - T_W(X)]$, so that $\theta_g(X,0) = \theta_s(X,0) = 0$ and $\theta_g(X,H) = 1$; then (7a) and (7b) appear as follows:

$$\frac{\partial^2\theta_s}{\partial y^2} - \frac{4Nu_d\kappa}{\delta^2}(\theta_s - \theta_g) = 0, \tag{8a}$$

$$\frac{\partial^2\theta_g}{\partial y^2} - \frac{4Nu_d\sigma}{\delta^2(1-\sigma)}(\theta_g - \theta_s) = -F(X)u(y), \tag{8b}$$

$$F(X) \equiv Re_H Pr\frac{\partial T_g/\partial X}{(T_W - T_H)/H} = Re_H Pr\frac{dT_{g,A}/dX}{(T_W - T_H)/H},$$

where $F(X)$ is a parameter to be determined which results in a Nusselt number expression (similar to K_L for the friction factor), and where $T_{g,A}$ is the bulk-average gas temperature. Here, the second equality for F applies for the case of constant wall heat-flux ($q_W = \text{const.}$) so that F is also constant. With $r_s \equiv \sigma/[\kappa(1-\sigma)]$, (8a) and (8b) can be combined to yield

$$\frac{\partial^2}{\partial y^2}(\theta_g + r_s\theta_s) = -Fu(y). \tag{8c}$$

The complete solution of (8a)–(8c) requires the local fiber-diameter Nusselt number, $Nu_d = hd/k_g$, usually as a function of the local Reynolds number, $Re_d = \rho Ud/\mu = (\rho U_H H/\mu)(d/H)(U/U_H) = Re_H\delta u(y)$. Numerous correlations have been reported for $Re_d > 0.4$, such as by Hilpert [9], Whitaker [10], Zhukauskas [11], Nakai and Okazaki [12], Churchill and Bernstein [13], Fowler and Bejan [2], Kang et al. [14]; some of these can also be found in recent texts [7,15,16].

The extrapolation of these correlations to small fiber Reynolds numbers is shown in Fig. 2(b). It is seen that the Fowler and Bejan correlation [2] over-estimates the single-cylinder results for the sparse packing of $\sigma = 1\%$, and that the Whitaker correlation [10] under-estimates the other results for the low Re_d values. Both the Hilpert [9] and Zhukauskas [11] correlations extrapolate to low values at the lowest Re_d shown, whereas the correlations of Churchill and Bernstein [13], Nakai and Okazaki [12], and Kang et al. [14] extend to a similar constant Nu_d value.

In view of these variations and lack of experimental data for small Reynolds numbers, it is here considered adequate to treat Nu_d as a parameter evaluated at $y = 1$. Let $\Omega^2 \equiv 4Nu_d\kappa(1 + r_s)$, and $\psi \equiv \theta/F$, then the fiber region energy Eqs. (8a) and (8b) become

$$\delta^2\frac{\partial^2\psi_s}{\partial y^2} - \frac{\Omega^2}{1+r_s}(\psi_s - \psi_g) = 0, \tag{9a}$$

$$\delta^2\frac{\partial^2\psi_g}{\partial y^2} - \frac{\Omega^2 r_s}{1+r_s}(\psi_g - \psi_s) = -\delta^2 u(y). \tag{9b}$$

2.4. Central core region heat transfer

In the fiber-free central region of a circular duct, the energy equation is

$$\frac{1}{R}\frac{\partial}{\partial R}\left\{R\frac{\partial T_C}{\partial R}\right\} = \frac{U_C}{\alpha_g}\frac{\partial T_C}{\partial X} \tag{10a}$$

or, in scaled terms, for both circular and planar ducts

$$\frac{1}{(\beta-y)^n}\frac{\partial}{\partial y}\left\{(\beta-y)^n\frac{\partial\theta_C}{\partial y}\right\}=-Fu_C. \tag{10b}$$

Then, the average temperature is given by

$$\theta_A=\frac{2^n}{u_A\beta}\left\{\int_0^1 u\theta_g\,dy+\int_1^\beta u_C\theta_C(1-y/\beta)^n\,dy\right\}. \tag{10c}$$

3. Solution of equations

3.1. Velocity and friction factor solutions

For the *fiber region*, because $\varepsilon\ll 1$, it is convenient to treat the linearized momentum Eq. (3c) as a singular perturbation problem, as previously [17,18] (even though the exact solution is available). Then as $\varepsilon\to 0$, the *outer* solution of (3c) (for the fiber mid-section) is, simply, the constant velocity, $u^\circ=K_L$. Two *inner* solutions exist: one for the top with $\eta=(1-y)/\varepsilon$, and one for the bottom with $\eta=y/\varepsilon$; both regions are described by

$$\frac{d^2u}{d\eta^2}-\omega^2u=-\omega^2K_L. \tag{11a}$$

The solution of (11a) is

$$u^{b,t}=a_{b,t}e^{-\omega\eta}+K_L, \tag{11b}$$

where (to satisfy boundary conditions) for the bottom of the fibers $a_b=-K_L$, and for the top $a_t=1-K_L$. Thus, the combined, inner/outer perturbation velocity solution for the fiber region is

$$u=e^{-\omega(1-y)/\varepsilon}+K_L\left(1-e^{-\omega y/\varepsilon}-e^{-\omega(1-y)/\varepsilon}\right). \tag{11c}$$

Hence, for any $y\neq 0$ or 1, $u\to K_L$ as $\varepsilon\to 0$; $u=0$ for $y=0$; and $u=1$ for $y=1$. The velocity profiles from (11c) are plotted in Fig. 3 for several values of ε (with $K_L=2\varepsilon$); it is seen that velocity "hold-up" and fiber drag are substantial for small ε, but less in comparison to viscous forces for larger ε values. The perturbation solutions in Fig. 3 were found to agree with exact solutions for ε-values below 0.3. The velocity gradient from (11c) becomes steep for $y=1$ as $\varepsilon\to 0$

$$\frac{du}{dy}=\frac{\omega}{\varepsilon}\left[(1-K_L)e^{-\omega(1-y)/\varepsilon}+K_Le^{-\omega y/\varepsilon}\right]\to\frac{\omega}{\varepsilon}(1-K_L)\text{ as }y\to 1. \tag{11d}$$

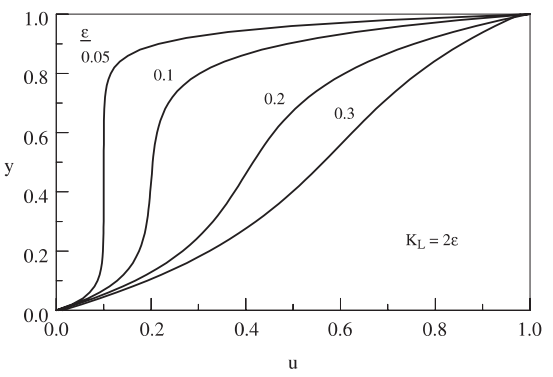

Fig. 3. Fiber region velocity distributions.

For the *core region*, the first and second integrals of (4b) are

$$\frac{du_C}{dy}=\frac{Re_Hf_H}{2(n+1)}(\beta-y)\to\frac{Re_Hf_H}{2(n+1)}(\beta-1)\text{ as }y\to 1, \tag{12a}$$

$$u_C=1+\frac{Re_Hf_H}{4(n+1)}(y-1)[2(\beta-1)-(y-1)]. \tag{12b}$$

Therefore, from (5), (11c) and (12b), and for $\varepsilon\to 0$, the average velocity over the circular duct is

$$\beta^2u_A=2\beta\left[K_L+\frac{\varepsilon}{\omega}(1-2K_L)\right]+(\beta-1)^2\left[1+\frac{Re_Hf_H}{16}(\beta-1)^2\right] \tag{13a}$$

and over the planar duct is

$$\beta u_A=\left[K_L+\frac{\varepsilon}{\omega}(1-2K_L)\right]+(\beta-1)\left[1+\frac{Re_Hf_H}{6}(\beta-1)^2\right]. \tag{13b}$$

For a circular duct, $\beta=1$ is *not* admissible; however, in both (13a) and (13b) it is seen that as $\beta\to 1$ (fibers fill more of the duct), the average velocity is computed mostly from the fiber region terms, whereas for large β (small fiber lengths) the core-terms matter most.

The fluid shear forces (shear stress times area) at the fiber/core interface must match: $(1-\sigma)\tau_H^-=\tau_H^+$, or at $y=1$, $(1-\sigma)\,du/dy=du_C/dy$. This results in

$$\frac{\omega(1-\sigma)}{\varepsilon}[1-K_L]\equiv\frac{\omega(1-\sigma)}{\varepsilon}\left[1-\frac{1}{10}-\frac{\varepsilon K_H}{\omega^2}+\frac{\lambda}{4\omega^2}\right]=\frac{Re_Hf_H}{2(n+1)}(\beta-1) \tag{14a}$$

but, by definition, $K_H\equiv\varepsilon Re_Hf_H/2(1-\sigma)$; thus, from (14a), K_H is O(1) as follows:

$$K_H=\frac{\omega(n+1)(9/10+\lambda/4\omega^2)}{\beta-1+\varepsilon(n+1)/\omega}\approx\frac{\omega(n+1)}{\beta-1}\left(\frac{9}{10}+\frac{\lambda}{4\omega^2}\right)\left(1-\frac{\varepsilon}{\omega}\frac{n+1}{\beta-1}\right) \tag{14b}$$

and $Re_Hf_H=2(1-\sigma)K_H/\varepsilon$ is a large number. Now, from (1a) $f_H=u_A^2fH/D$, and by definition $Re_H=$

$(Re/u_A)H/D$; therefore, $Re_H f_H = Re f u_A (H/D)^2$ and $u_A = 2K_H(D/H)^2(1-\sigma)/(\varepsilon Re \cdot f)$; combining this result with (13a) and (13b) we find the expression for the $Re \times f$ product for a *circular* duct with short fibers

$$\frac{64}{Ref} = (1-1/\beta)^4\left\{1+\frac{\varepsilon}{\omega}\frac{40/9}{(1-\sigma)(\beta-1)}+\cdots\right\} + \frac{\varepsilon}{\omega}\frac{8}{9}\frac{\beta-1}{(1-\sigma)\beta^3}+\cdots \tag{14c}$$

and for a *plane* duct

$$\frac{96}{Ref} = (1-1/\beta)^3\left\{1+\frac{\varepsilon}{\omega}\frac{10/3}{(1-\sigma)(\beta-1)}+\cdots\right\} + \frac{\varepsilon}{\omega}\frac{1}{3}\frac{\beta-1}{(1-\sigma)\beta^3}+\cdots \tag{14d}$$

Thus, it is seen that $Re \times f \to (Re \times f)_{\text{smooth}}$ as $1/\beta \to 0$ for both the plane and round ducts (i.e., as the fibers disappear). These Reynolds-friction products from (14c) and (14d) are shown in Fig. 4 as functions of the fiber length, relative to the duct half-width or radius. It is seen that the multiplier increases rapidly as the duct becomes progressively filled with fibers, but that for $1/\beta < 0.3 (\beta > 3)$ the friction multiplier is limited to less than about 3. Hence, there is substantially lower friction and pressure drop when fibers are limited to the wall region.

3.2. Fiber region heat transfer solution

For the fiber region, (8c) and (11c) combine to yield the first integral

$$\frac{\partial}{\partial y}\left(\theta_g + r_s\theta_s\right) = -F(X)\int u\,dy + C_1(X) \tag{15a}$$

with

$$\int u\,dy = \frac{\varepsilon}{\omega}(1-K_L)e^{-\omega(1-y)/\varepsilon} + K_L\left(y+\frac{\varepsilon}{\omega}e^{-\omega y/\varepsilon}\right).$$

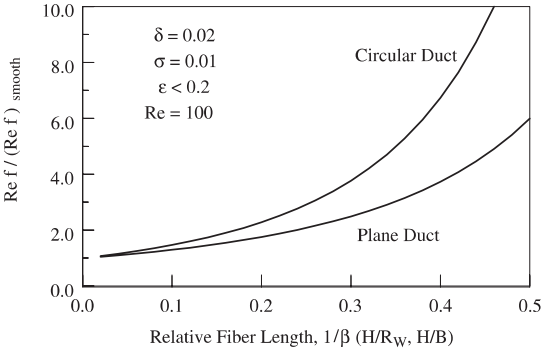

Fig. 4. Friction factor multipliers.

At the wall, $q_W = (1-\sigma)q_{W,g} + \sigma q_{W,s}$; with the Fourier conduction relation this leads to the requirement

$$(1-\sigma)\left.\frac{\partial\theta_g}{\partial y}\right|_{y=0} + \frac{\sigma}{\kappa}\left.\frac{\partial\theta_s}{\partial y}\right|_{y=0} = \frac{1}{n+1}\beta u_A F \tag{15b}$$

so that with (13a), (13b) and (15a), $C_1 = [\beta u_A/(n+1)(1-\sigma) + \varepsilon K_L/\omega]F$. Thus, the sum-of-flux equation is

$$\frac{\partial}{\partial y}\left(\theta_g + r_s\theta_s\right) = \left(\frac{\beta u_A}{(n+1)(1-\sigma)} - K_L y + \frac{\varepsilon}{\omega}\left[(1-K_L)e^{-\omega(1-y)/\varepsilon} + K_L\left(1-e^{-\omega y/\varepsilon}\right)\right]\right)F(X). \tag{15c}$$

A further integration of (15c) yields

$$\theta_g + r_s\theta_s = \left[\left(\frac{\beta u_A}{(n+1)(1-\sigma)}\right)y - K_L\frac{y^2}{2} + \frac{\varepsilon}{\omega}K_L + O(\varepsilon^2)\right]F(X) + C_2(X). \tag{15d}$$

Because both nondimensional temperatures are zero at $y=0$, $C_2 = 0$. For the tip condition of the fibers, H is taken such that the usual fin extension is included [7] and such that $[d\theta_s/dy]_{y=1} = 0$; therefore, (15c) yields the expression for F

$$F = \frac{\left[\partial\theta_g/\partial y\right]_{y=1}}{\gamma}, \qquad \gamma \equiv \frac{\beta u_A}{(n+1)(1-\sigma)} - K_L + \varepsilon/\omega + \cdots \tag{15e}$$

Now, substitution of (15d) into (9a) yields a single equation for integration

$$\delta^2\frac{\partial^2\psi_s}{\partial y^2} - \Omega^2\psi_s = -\frac{\Omega^2}{1+r_s}\left\{\left(\frac{\beta u_A}{(n+1)(1-\sigma)} + \frac{\varepsilon}{\omega}K_L\right)y - K_L\frac{y^2}{2}\right\}. \tag{16}$$

Because $\delta \ll 1$, (16) is also a singular perturbation equation. Thus, the outer solution is

$$\psi_s^\circ = \frac{1}{1+r_s}\left\{\left(\frac{\beta u_A}{(n+1)(1-\sigma)} + \frac{\varepsilon}{\omega}K_L\right)y - K_L\frac{y^2}{2}\right\}. \tag{17a}$$

Since this goes to 0 for $y=0$, there is no thermal boundary layer at the wall. For the fiber-tip region we take $\zeta = (1-y)/\delta$; then the inner solution of (16) is of the form $e^{-\Omega\zeta}$, and the outer plus inner solution is

$$\psi_s = \frac{1}{1+r_s}\left\{\left(\frac{\beta u_A}{(n+1)(1-\sigma)} + \frac{\varepsilon}{\omega}K_L\right)y - K_L\frac{y^2}{2} + b_s e^{-\Omega(1-y)/\delta}\right\} \tag{17b}$$

setting the slope of (17b) to zero at $y = 1$, we have $b_s = (\delta/\Omega)[K_L - \beta u_A/(n+1)(1-\sigma)]$. Therefore, the solution of (16) gives the solid temperature as

$$\psi_s = \frac{1}{1+r_s}\left\{\frac{\beta u_A}{(n+1)(1-\sigma)}\left(y - \frac{\delta}{\Omega}e^{-\Omega(1-y)/\delta}\right) - K_L\left(\frac{y^2}{2} - \frac{\varepsilon}{\omega}y - \frac{\delta}{\Omega}e^{-\Omega(1-y)/\delta}\right)\right\} \quad (17c)$$

and with (15d) the fluid temperature is

$$\psi_g = \frac{1}{1+r_s}\left\{\frac{\beta u_A}{(n+1)(1-\sigma)}\left(y + \frac{\delta r_s}{\Omega}e^{-\Omega(1-y)/\delta}\right) - K_L\left(\frac{y^2}{2} + \frac{\varepsilon r_s}{\omega}y + \frac{\delta r_s}{\Omega}e^{-\Omega(1-y)/\delta}\right)\right\}. \quad (17d)$$

Therefore, since $\psi_g(1) = 1/F$, or $\theta_g(1) = 1$, we have

$$\frac{1+r_s}{F} = \frac{\beta u_A}{(n+1)(1-\sigma)}\left(1 + \frac{\delta r_s}{\Omega}\right) - K_L\left(\frac{1}{2} + \frac{\varepsilon r_s}{\omega} + \frac{\delta r_s}{\Omega}\right). \quad (17e)$$

This completes the fiber region thermal solution; a typical solution is shown in Fig. 5 where θ_g and θ_s are plotted versus y on the abscissa. There tends to be little temperature difference between the fibers and fluid near $y = 0$, but farther towards the tips of the fibers, there is greater temperature difference and heat transfer from the solid to the fluid, for further conduction to the core flow; this is especially so for large fiber conductivities ($\kappa \to 0$), as seen. The slope of θ_s at $y = 1$ is zero, as required, with θ_s progressively smaller for larger fiber conductivities; for each curve, $\theta_g(1) = 1$, as required.

3.3. Core region heat transfer solution

In a smooth duct with a diameter or half-width equivalent to the fiber-free central core region, the fully developed Nusselt number is given by [8]

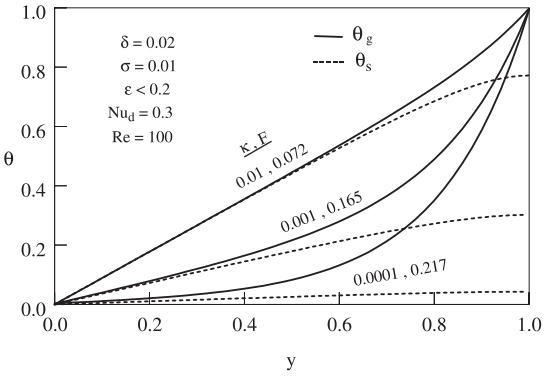

Fig. 5. Fiber region temperature distributions.

$$Nu_m \equiv \frac{h_m D_m}{k_g} = \frac{[q_H(1-\sigma)/(T_H - T_m)][(R_W - H)4/(n+1)]}{k_g} = \frac{H(1-\sigma)(\beta-1)4/(n+1)}{k_g[(T_H - T_W) - (T_m - T_W)]}\left(-k_g\frac{\partial T_g}{\partial Y}\right)_{Y=H} = -\frac{4}{n+1}\frac{(1-\sigma)(\beta-1)}{1-\theta_m}\frac{\partial\theta_g}{\partial y}\bigg|_{y=1}. \quad (18a)$$

This Nu/temperature-gradient relationship also holds under translation of bulk and wall velocities of the equivalent duct, and so applies to the core region of the present geometries. Thus, combining (15e) and (18a), the mean temperature is

$$\theta_m = 1 + \frac{4}{n+1}\frac{\gamma F}{Nu_m}(\beta-1)(1-\sigma) = 1 + \frac{2(\beta-1)}{n+1}\frac{F}{Nu_m}[\beta u_A - 2(1-\sigma)(K_L - \varepsilon/\omega)]. \quad (18b)$$

Since for a pipe with constant boundary heat flux, $Nu_m = 4.36$ ($= 8.23$ for a plane duct), the mixed mean temperature is a known quantity from (18b). Substantially the same results were obtained by integration over the core using a symbolic math processor, but expressed in a much more complicated form.

3.4. Duct Nusselt number

Let subscript A denote the mixed-mean average over the entire cross-section, then with $\theta_A = (T_A - T_W)/(T_H - T_W)$, the bulk-average duct temperature is

$$\theta_A = \frac{1}{u_A}\left\{\frac{n+1}{\beta}I_1 + (1-1/\beta)^{n+1}u_m\theta_m\right\}, \quad (19a)$$

where, from (13a) for a circular duct

$$u_m = (1-1/\beta)^2\left[1 + \frac{u_A Ref}{64}(1-1/\beta)^2\right] \quad (19b)$$

and, from (13b) for a planar duct

$$u_m = (1-1/\beta)\left[1 + \frac{u_A Ref}{96}(1-1/\beta)^2\right], \quad (19c)$$

where the integral, I_1, is

$$I_1 = \frac{F}{1+r_s}\left\{K_L\left(\frac{a_1}{2} + \frac{a_2}{3} + b\frac{\delta}{\Omega}\right) + \frac{\varepsilon}{\omega}(K_L - 1) \times\left(a_1 + a_2 + b\frac{\delta\omega}{\delta\omega + \varepsilon\Omega}\right)\right\} \quad (19d)$$

and where

$$a_1 = B_1 - K_L r_s\varepsilon/\omega,\ B_1 = \beta u_A/(1-\sigma),\ a_2 = -K_L/2,$$
$$b = (B_1 - K_L)r_s\delta/\Omega.$$

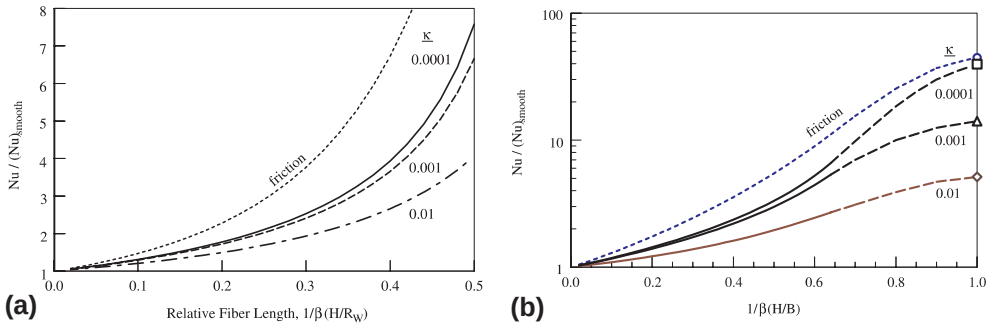

Fig. 6. (a) Nusselt number multipliers for circular duct. (b) Nusselt number multipliers for planar duct.

But, considering overall energy balance, with the definition of the wall heat transfer coefficient and of F, the Nusselt number is defined as

$$Nu_A \equiv \left(\frac{2}{n+1}\right)^2 \frac{\beta^2 u_A F}{\theta_A}. \tag{20a}$$

Therefore, we have the expression for the bulk-average Nusselt number

$$Nu_A = \left(\frac{2}{n+1}\right)^2 \frac{\beta^2 u_A^2 F}{(n+1)I_1/\beta + (1-1/\beta)^{n+1} u_m \theta_m} = \frac{(2/(n+1))^2 \beta^2 u_A^2 F}{(n+1)I_1/\beta + (1-1/\beta)^{n+1} u_m [1 + 4(\beta-1)(1-\sigma)\gamma F/(n+1)Nu_m]} \tag{20b}$$

or, with the definition of γ, the (inverse) Nusselt number multiplier is

$$\frac{Nu_m/u_m}{Nu_A/u_A} = \left(1-\frac{1}{\beta}\right)^{n+2} \left\{1 + \frac{n+1}{\beta u_A F}\left[\frac{n+1}{4}\frac{Nu_m}{\beta-1} - F(1-\sigma)\left(K_L - \frac{\varepsilon}{\omega}\right)\right]\right\} + \frac{(n+1)^3 Nu_m/u_m}{4\beta^3 u_A F} I_1. \tag{20c}$$

It is seen in (20a)–(20c) that $Nu_A \to Nu_m$ as $\beta \to \infty$ (no fibers), as expected.

For the *circular* duct ($n = 1$), the Nusselt number multiplier, m_h, from (20c) is shown in Fig. 6(a), with κ as a parameter. It is seen that m_h starts out at 1 for no fibers, but then increases rapidly for progressively longer fibers, similarly as the friction multiplier, m_f; high-conductivity fibers have greater rates of increase than do those of lower values. The m_h multiplier increase is substantial: for $m_f \approx 3$, it is possible to have $m_h > 2$ for any laminar Reynolds number. This performance is typical of conventional surface roughness in turbulent flow, but difficult to achieve for laminar flow [3,4]; indeed, $m_h \approx 2$ appears to be an upper limit for rectangular roughness in turbulent flow, but approaching laminar flow this enhancement disappears [4]. By contrast, the present fiber "roughness" predicts an m_h as large as 8 for fiber lengths of half the radius, albeit at about twice the friction factor penalty. Thus, much larger heat transfer coefficients are possible with fiber-flocked surfaces in laminar flow than hitherto with conventionally rough surfaces; this conclusion is expected to extend to turbulent flow, as well.

For the *planar* duct ($n = 0$), a similar behavior is shown in Fig. 6(b) on a logarithmic scale, but here the fibers can extend to the centerline and altogether eliminate the core. Data points were calculated for this case, shown as the symbols in Fig. 6(b) for $1/\beta = 1$, and the present results extrapolated thereto by the dashed lines. It is seen that very substantial heat transfer enhancements are possible.

In these calculations, the fiber-tip velocity, U_H, varies with β even though the bulk Reynolds number is constant. Therefore, for the Fig. 6 curves, the fiber-diameter Nusselt number was evaluated using the Nakai and Okazaki correlation [12]: $Nu_d = 1/[0.8237 - 0.5\ln(Re_{d,H}Pr)]$, with $Re_{d,H} = \rho U_H d/\mu$.

The surface heat transfer coefficient determined from the above results is for perfect fiber conductance to the wall ($h_{c,w} \to \infty$), as can be achieved by soldering and other processes. This can be corrected for finite contact conductance as follows, $1/h'_A = 1/h_A + 1/h_{c,w}$, where the prime denotes the corrected heat transfer coefficient; here, $h_{c,w} = \sigma \times h_{c,s}$ and $h_{c,s} = S \times k_c/d$ are the effective fiber-contact conductances based respectively on the entire wall and fibers cross-section areas, and S is the shape factor [7]. For example, for an unfilled polymer adhesive of conductivity $k_c = 0.2$ W/mK, a fiber diameter of $d = 10$ μm, and a packing fraction of $\sigma = 0.10$, it was found experimentally that $h_{c,w} \approx 20,000$ W/m^2 K; thus, $h_{c,s} \approx 200,000$ W/m^2 K and $S \approx 10$. Effective contact design is achieved for $Bi_c \geqslant 1$, where the contact Biot number is $Bi_c \equiv h_{c,s}H/k_s = S(H/d)(k_c/k_s)$.

4. Conclusion

An analysis has been performed for fully developed laminar flow and heat transfer in plane and cylindrical

ducts having fine, high-conductivity fibers sparsely attached to the walls. The model equations, based on correlations from the literature, were solved by singular perturbation theory, with performance results stated in analytical terms. The results are in terms of friction factor and Nusselt number multipliers, which are constant for all laminar Reynolds numbers, but which vary strongly with the fiber conductivity and length, relative to the duct half-width or radius. At larger fiber conductivities and lengths, the results indicate greater heat transfer enhancements than hitherto possible in laminar flow.

Acknowledgements

The present work was generously supported by a research gift from Energy Science Laboratories, Inc. to the University of California, San Diego.

References

[1] A. Bejan, Theory of heat transfer from a surface covered with hair, J. Heat Transfer 112 (1990) 662–667.
[2] A.J. Fowler, A. Bejan, Forced convection from a surface covered with flexible fibers, Int. J. Heat Mass Transfer 38 (1995) 767–777.
[3] J.Y. Yun, K.S. Lee, Investigation of heat transfer characteristics on various kinds of fin-and-tube heat exchangers with interrupted surfaces, Int. J. Heat Mass Transfer 42 (1999) 2375–2385.
[4] R. Karwa, S.C. Solanki, J.S. Saini, Heat transfer coefficient and friction factor correlations for the transitional flow regime in rib-roughned rectangular ducts, Int. J. Heat Mass Transfer 42 (1999) 1597–1615.
[5] H. Schlichting, Boundary Layer Theory, McGraw-Hill, New York, 1968.
[6] F.M. White, Viscous Fluid Flow, McGraw-Hill, New York, 1974.
[7] F.P. Incropera, D.P. DeWitt, Fundamentals of Heat and Mass Transfer, IV ed., Wiley, New York, 1996.
[8] W.M. Kays, M.E. Crawford, Convective Heat and Mass Transfer, II ed., McGraw-Hill, New York, 1980.
[9] R. Hilpert, Forsch. Geb. Ingenieurwes. 4 (1933) 215.
[10] S. Whitaker, Forced convection heat transfer correlations for flow in pipes past flat plates, single cylinders single spheres, and flow in packed beds and tube bundles, AIChE J. 18 (1972) 361–371.
[11] A. Zhukauskas, Heat transfer from tubes in cross flow, in: J.P. Hartnett, T.F. Irvine (Eds.), Advances in Heat Transfer, vol. 8, Academic Press, New York, 1972.
[12] S. Nakai, T. Okazaki, Heat transfer from a horizontal circular wire at small Reynolds and Grashof numbers – 1 pure convection, Int. J. Heat Mass Transfer 18 (1975) 387–396.
[13] S.W. Churchill, M. Bernstein, A correlating equation for forced convection from gases and liquids to a circular cylinder in crossflow, J. Heat Transfer, Trans. ASME Ser. C 99 (1977) 300–306.
[14] S.-H. Kang, K.-H. Hong, S. Kauh, A unified correlation of laminar convective heat transfer from hot and cold circular cylinders in a uniform air flow, Int. J. Heat Mass Transfer 38 (1995) 752–755.
[15] F.M. White, Heat and Mass Transfer, Addison-Wesley, New York, 1988.
[16] J.H. Lienhard, Heat Transfer Textbook, second ed., Prentice-Hall, Englewood Cliffs, NJ, 1987.
[17] K.O. Lund, W.B. Bush, Asymptotic analysis of plane turbulent Couette–Poiseuille flows, J. Fluid Mech. 96 (part 1) (1980) 81–104.
[18] K.O. Lund, Asymptotic analysis of turbulent flow for a rotating cylinder, in: K. Gersten (Ed.), Proceedings of the International Union of Theoretical and Applied Mechanics: Symposium on Asymptotic Methods for Turbulent Shear Flows at High Reynolds Numbers, Kluwer Academic Publishers, Dordrecht, 1996, pp. 45–58.